Structure Dependence of Free-Charge Transfer in Charge-coupled Devices

Abstract: A detailed numerical analysis of charge-coupled-device (CCD) charge transfer is described and discussed. The analysis is based on solving the transport equation with a time-dependent surface field calculated from the actual device configuration. Devices with different oxide thicknesses and devices with electrode gaps are examined. The total field is found to play an important role in charge transfer for all cases studied. The effective channel length is modulated by the net field present and is a function of time and electrode configuration. The transfer is found fastest and the effective channel length shortest when the charge is transferred from a region of low oxide capacitance into a region of high oxide capacitance. A low-capacitance electrode gap slows the charge transfer process.

Introduction

The charge-coupled device (CCD), since its introduction by Bell Laboratories [1], has generated much theoretical and experimental interest [2-15]. It has been demonstrated to be useful in high density memory [16-20] and in image sensing [21, 22]. The device operates by moving minority carriers along a series of potential wells formed by a metal-oxide-semiconductor (MOS) array. Strain and Schryer [2] used a simplified transport equation and simplified boundary conditions to show that the transfer of minority carriers takes place initially due to a self-induced drifting field and later by a diffusion process. That analysis neglected any fringe field due to adjacent electrodes. Heller, Chang and Lo [4] later assumed a constant fringe field and showed that the transfer characteristics of the device can be modified significantly by the inclusion of the fringe field. Mohsen et al. [15], Amelio [23], and Carnes et al. [24] extended the analysis by including an approximate fringe field. However, in this work, we conclude that the amount of charge-induced field and the amount of fringe field both depend on the actual electrode configuration and that both are functions of time. We use a numerical method to realistically calculate the transfer characteristics of CCD devices. The analysis includes both devices with different oxide thicknesses and devices with electrode gaps. No attempt is made to differentiate between the effect of the chargeinduced field and the effect of the fringe field due to adjacent electrodes. The time-dependent total field that must be calculated depends on both the charge distribution and the electrode configuration. As a consequence, different electrode configurations have different effects on the CCD charge transfer characteristics. With proper design,

the total field modulates the effective device channel length and speeds up charge transfer. The effect of surface states is not considered in this paper.

Mathematical analysis

A general form of a CCD structure is shown in Fig. 1. Assume that the minority carriers per unit area, $n^*(x^*, t^*)$ (an asterisk is used to represent unnormalized quantities), flow along the silicon surface within a channel of infinitesimal thickness. The transport equations governing the transfer of minority carriers in the x^* direction are

$$q \frac{\partial n^*}{\partial t^*} = \frac{\partial J^*}{\partial x^*}$$
, and (1)

$$J^{*}(x^{*}, t^{*}) = q\mu^{*} \left\{ \frac{kT}{q} \frac{\partial n^{*}}{\partial x^{*}} + n^{*}E_{s}^{*} \right\}, \tag{2}$$

where J^* is the current density per unit width perpendicular to the direction of carrier flow and μ^* is the carrier mobility. The surface tangential electric field, $E_s^*(x^*, t^*)$, is determined by solving the two-dimensional boundary value problem defined by the following equations [25]:

$$\nabla^{*2} \phi^* = 0; \ y^* \ge 0, \tag{3}$$

$$\nabla^{*2}\phi^* = -\frac{\rho^*}{\varepsilon_{\text{si}}^*}; \, y^* \le 0, \tag{4}$$

$$\rho^*(x^*, y^*, t^*) = q\{N_{AB}^* \exp(-q\phi^*/kT) - N_A^*(x^*, y^*) + \delta(y^*)[N_A^*(x^*) - n^*(x^*, t^*)]\}, \quad (5)$$

and

$$E_{s}^{*}(x^{*}, t^{*}) = -(\partial \phi^{*}/\partial x^{*})|_{u=0}^{*},$$
(6)

with the boundary conditions

$$\phi^*(x^*, y^*, t^*) = 0 \text{ at } [x^{*2} + y^{*2}]^{\frac{1}{2}} = \infty;$$
 (7)

$$\phi^*(x^*, y^*, t^*) = V_i^{\prime *}(t^*) - \phi_{MS}^*$$

$$= V_i^{\ast}(t^*) \text{ on the } i\text{th electrode,}$$
 (8)

where q is the electronic charge, k is Boltzmann's constant, T is the absolute temperature, $\phi^*(x^*, y^*, t^*)$ is the potential at time t^* , N_A^* and N_{AB}^* are doping densities at (x^*, y^*) and $(x^*, y^* = -\infty)$ respectively, and ϕ_{MS}^* is the work function difference between the metal and the bulk substrate at $y^* = -\infty$. $N_s^*(x^*)$ is the effective immobile surface charge density and is assumed to be time independent. Also, $\delta(y^*)$ is the Dirac delta function, and ε_{Si}^* and ε_{Ox}^* are the permittivities of silicon and oxide, respectively.

On the Si-SiO₂ interface $y^* = 0$, and both the potential and the tangential electric field are continuous, whereas the normal component of the displacement vector is discontinuous by the amount of surface charge associated with mobile carriers and the surface states. We have assumed that the substrate is p-type with doping density $N_A^*(x^*, y^*)$. The *i*th electrode is W_i^* in width, h_i^* above the silicon surface and is driven by a pulse voltage V_i^* as shown in Fig. 1. The upper and lower half space are filled with SiO₂ and Si, respectively. In writing Eq. (5) we have neglected the bulk minority carriers and assumed that the bulk majority carriers are in thermal equilibrium at all times under pulse voltage operation. The mobility μ^* is assumed to be constant μ_0^* .

Equations (1) to (8) can be normalized by defining

$$\lambda_{D} = \left[\left(\varepsilon_{Si}^{*} kT \right) / \left(q^{2} N_{AB}^{*} \right) \right]^{\frac{1}{2}}; x = x^{*} / \lambda_{D}; y = y^{*} / \lambda_{D};$$

$$\phi = \frac{\phi^{*}}{kT/q}; V_{i} = \frac{V_{i}^{*}}{kT/q};$$

$$N_{A} = \frac{N_{A}^{*}}{N_{AB}^{*}}; N_{S} = \frac{N_{S}^{*}}{\lambda_{D} N_{AB}^{*}};$$

$$n = \frac{n^{*}}{\lambda_{D} N_{AB}^{*}}; \varepsilon = \frac{\varepsilon_{OX}^{*}}{\varepsilon_{Si}^{*}}; \text{ and}$$

$$\tau = \left(\frac{\mu_{0}^{*} kT}{\lambda_{D}^{*} q} \right) t. \tag{9}$$

Then the normalized equations become

$$\frac{\partial n}{\partial \tau} = \frac{\partial J}{\partial x} \,, \tag{10}$$

$$J = \mu \left(\frac{\partial n}{\partial x} - n \, \frac{\partial \phi_{\rm s}}{\partial x} \right),\tag{11}$$

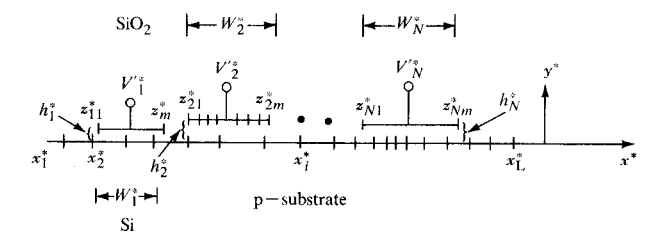


Figure 1 A schematic representation of the structure of a charge-coupled device.

$$\nabla^2 \phi = 0; y \ge 0, \tag{12}$$

$$\nabla^2 \phi = -\rho; \ y \le 0, \tag{13}$$

$$\rho = \exp(-\phi) - N_{A}(x, y) + \delta(y)[N_{S}(x) - n], \tag{14}$$

$$\phi_{s} = \delta(x, 0, t), \tag{15}$$

$$\phi = 0$$
 at $(x^2 + y^2)^{\frac{1}{2}} = \infty$, and (16)

$$\phi = V_i$$
 on the *i*th electrode. (17)

To obtain the complete solution, Eqs. (10) through (17) must be solved simultaneously. Even through the use of a modern high speed computer, this calculation is a rather time consuming process. To speed up the solution, the following procedures are followed. Equations (12) through (17) are solved by initially assuming a given charge distribution. The resulting bulk charge and the surface potential are used as the initial conditions for Eq. (10), which is then solved by assuming that the bulk charge does not change during the short time period over which the solution is being calculated. The surface potential, however, is continuously calculated by taking into account the variation of surface charge and the electrode charge. After a short period of time, Eqs. (12) through (17) are re-solved to obtain a new bulk charge distribution by using the previously obtained surface charge. The process is repeated by alternating between the solution of Eq. (10) and the solution of Eqs. (12) through (17). The time interval consumed in recalculating the bulk charge is kept short so that a good approximation can be obtained. Because the calculation of bulk charge is made only a few times, a considerable saving in computing time is obtained.

The potential ϕ in the upper half space can be expressed as [25]

$$\phi(x, y, \tau) = \sum_{i=1}^{N} \int_{z_{i1}}^{z_{im}} q_i(x', \tau) G_{11}(x, y|x', h_i) dx'$$

$$- \int_{-\infty}^{\infty} n(x', \tau) G_{12}(x, y|x', 0) dx'$$

$$+ \phi_{BS}(x, y, \tau), \text{ where}$$
(18)

SEPTEMBER 1974

$$\begin{split} \phi_{\rm BS}(x,y,\tau) &= \int_{-\infty}^{\infty} N_{\rm s}(x') \ G_{12}(x,y|x',0) \ dx' \\ &+ \int_{-\infty}^{0} \int_{-\infty}^{\infty} \left\{ \exp[-\phi(x',y',\tau)] \right. \\ &- N_{\rm A}(x',y') \right\} \ G_{12}(x,y|x',y') \ dx' \ dy', \end{split}$$

$$G_{11}(x, y|x', y') = -\frac{1}{4\pi\varepsilon} \left\{ \ln[(x - x')^2 + (y - y')^2] - \frac{1 - \varepsilon}{1 + \varepsilon} \ln[(x - x')^2 + (y + y')^2] \right\};$$

$$y \ge 0; y' \ge 0, \tag{20}$$

$$G_{12}(x, y|x', y') = -\frac{1}{2\pi(1+\varepsilon)} \ln[(x-x')^{2} + (y-y')^{2}];$$

$$y \ge 0; y' \le 0.$$
 (21)

The electrode charges $q_i(x, \tau)$ and the minority charges $n(x, \tau)$ are approximated by piecewise-linear distributions, and the potential is given by

$$\phi(x, y, \tau) = \sum_{i=1}^{N} \sum_{k=1}^{m} q_{i,k}(\tau) A_{ik}(x, y) - \sum_{l=1}^{L} n_{l}(\tau) B_{l}(x, y) + \phi_{BS}(x, y, \tau)$$

$$= [A(x, y)]^{T} [q] - [B(x, y)]^{T} [n] + \phi_{BS}(x, y, \tau), \tag{22}$$

where $q_{i,k}(\tau)$ is the electrode charge density at $x=z_{i,k}$, $y=h_i$ and $n_l(\tau)$ is the minority charge density at $x=x_l$, y=0. Here, the boldface bracket, [] denotes the column matrix and T indicates the transpose. The matrix elements $A_{i,k}$ and B_l are

$$\begin{split} A_{i,k}(x,y) &= (1-\delta_{k1}) \int_{z_{i,k-1}}^{z_{i,k}} \frac{x'-z_{i,k-1}}{z_{i,k}-z_{i,k-1}} G_{11}(x,y|x',h_i) \ dx' \\ &+ (1-\delta_{km}) \int_{z_{i,k}}^{z_{i,k+1}} \frac{z_{i,k+1}-x'}{z_{i,k+1}-z_{i,k}} \\ &\times G_{11}(x,y|x',h_i) \ dx', \end{split} \tag{23}$$

$$B_{l}(x, y) = (1 - \delta_{l1}) \int_{x_{l-1}}^{x_{l}} \frac{x' - x_{l-1}}{x_{l} - x_{l-1}} G_{12}(x, y | x', 0) dx'$$

$$+ (1 - \delta_{lL}) \int_{x_{l}}^{x_{l+1}} \frac{x_{l+1} - x'}{x_{l+1} - x_{l}}$$

$$\times G_{12}(x, y | x', 0) dx'. \tag{24}$$

Here, δ_{kl} is the Kronecker delta function. The column matrix [q] can be obtained by requiring that (17) be satisfied at $x = x_{i,k}$, $y = h_i$, $i = 1, 2, \dots, N$, $k = 1, 2, \dots, m$. Or

$$[V] = [A_1][q] - [B_1][n] + [\phi_{BS1}], \text{ where}$$
 (25)

$$[V] = [V'_1, \dots, V'_1; V'_2, \dots, V'_2; V'_N, \dots, V'_N];$$

$$[A_1] = \begin{bmatrix} [A(z_{11}, h_1)]^T \\ \vdots \\ [A(z_{Nm}, h_N)]^T \end{bmatrix};$$

$$[B_1] = \begin{bmatrix} [B(z_{11}, h_1)]^T \\ \vdots \\ [B(z_{Nm}, h_N)]^T \end{bmatrix};$$

 $[\phi_{\rm BS1}] = [\phi_{\rm BS}(z_{11}, h_1, \tau), \cdots, \phi_{\rm BS}(z_{Nm}, h_N, \tau)]. \tag{26}$ Upon inverting,

$$[q] = [A_1]^{-1}[[V] + [B_1][n] - [\phi_{RS1}]]. \tag{27}$$

After substituting (27) into (22) and letting y = 0, we can express the surface potential in terms of bulk charges and the surface charges as

$$\phi_{S}(x,\tau) = \phi(x,0,\tau)$$

$$= [A(x,0)]^{T}[[A_{1}]^{-1}[V] + [B_{1}][n] - [\phi_{BS1}]]$$

$$- [B(x,0)]^{T}[n] + \phi_{BS}(x,0,\tau). \tag{28}$$

If the bulk charges remain unchanged during the period $\tau \ge \tau_0$, the surface potential at τ is given by

$$\begin{split} \phi_{\mathrm{S}}(x,\tau) &= \phi_{\mathrm{S}}(x,\tau_{0}) + [A(x,0)]^{\mathrm{T}} [A_{1}]^{-1} [V(\tau) - V(\tau_{0})] \\ &+ [[A(x,0)]^{\mathrm{T}} [A_{1}]^{-1} [B_{1}] \\ &- [B(x,0)]^{\mathrm{T}} [n(\tau) - n(\tau_{0})]] \\ &= \phi_{\mathrm{S}}(x,\tau_{0}) + [D(x)]^{\mathrm{T}} [V(\tau) - V(\tau_{0})] \\ &+ [G(x)]^{\mathrm{T}} [n(\tau) - n(\tau_{0})]. \end{split} \tag{29}$$

The column matrices D and G_1 are time independent, and Eq. (28) is used in conjunction with Eq. (11) to solve Eq. (10) during the period $\tau \ge \tau_0$. Approximate solutions to Eq. (10) can be presented in the following forms:

$$\begin{split} n_{l}(\tau+\Delta\tau) &= n_{l}(\tau) + \frac{\Delta\tau}{2} \; (x_{l+1}-x_{l-1}) \\ &\times \left\{ J\left(\frac{x_{l+1}+x_{l}}{2},\,\tau\right) - J\left(\frac{x_{l}+x_{l-1}}{2},\,\tau\right) \right\}; \quad (30) \\ J\left(\frac{x_{l+1}+x_{l}}{2},\,\tau\right) &= \frac{\mu}{x_{l+1}-x_{l}} \left\{ n_{l+1}(\tau) - n_{l}(\tau) - \frac{n_{l+1}+n_{l}}{2} \left[\phi_{s}(x_{l+1},\,\tau) - \phi_{s}(x_{l},\,\tau) \right] \right\}. \end{split}$$

Care has been taken so that the minority charges n_l would not become negative. If n_l is negative, it is reset to zero and the current J is adjusted so that the total amount of charges is conserved.

Numerical results

Based on the above approach, several calculated results are shown in Fig. 2. All electrodes are 5 μ m in width. The substrate is p-type and is doped uniformly with density $5 \times 10^{15} / \text{cm}^3$. The surface state charge density of the stepped-oxide devices is assumed to be $10^{11}/\text{cm}^2$. The minority carriers are assumed to be uniformly distributed under the first gate with concentration chosen such that the value Sq, defined in [2], is 10 V. The mobility is assumed to be 400 cm²/V-s. The transfer characteristic (curve a) calculated in [2] is included in the figure for comparison. Curve b, shows the transfer characteristic of the charges being transferred from thick oxide region (2000 Å) into thin oxide region (1000 Å). Because the field penetrates substantially deep under gate 1, the charge is swept out of gate 1 much faster than that without a fringe field (curve a). The time-dependent surface potential distribution is shown in Fig. 3. It is seen that the effective channel length is actually reduced and the charge reduces to a small value under the gate instead of at the edge of the electrode as commonly assumed. The bulk charge is recalculated in this case at times (all ns), t = 0, 0.051; 0.1, 0.2, 0.4, 0.8,and 2. After 2 ns the surface potential changes very little, indicating that the amount of charge left to be transferred is small. Therefore, no further recalculation of bulk charge is necessary to determine the transfer efficiency of the device. When the same amount of charge is initially stored under the thin oxide region, the transfer characteristic of the charge transferring into thick oxide region is given by curve b, (Fig. 2). The charge quickly fills up the potential well under gate 2 and leaves behind more than one fifth of the initial charge under gate 1. To have a complete transfer and to maintain $Sq_0 = 10 \text{ V}$, the initial charge density is changed to $1.66 \times 10^{12}/\text{cm}^2$ and the difference between the applied voltages is increased to 24 V instead of the 10 V used in case b,. Even with this large potential difference, the transfer (curve c₁) is slower than in case b₁. The reason is that the field, due to shielding associated with electrode 1, is smaller in this case. Figure 4 shows the surface potential profile as a function of time for c₁. The time indicated is the time at which the bulk charge is recalculated. The charge can be seen to approach a small value at a point closer to the edge of the electrode.

The effect of the amount of potential difference between the two neighboring potential wells can be seen on curves c_2 , c_3 and c_4 . The potential differences at t=2 ns (which is very close to the final potential difference when all charges are completely transferred) are about 2.9 V, 1.6 V, 0.8 V and 0.6 V, respectively, for curves c_1 , c_2 , c_3 and c_4 . When the two potential wells approach each other, the transfer slows down considerably. It is important to note that in cases c_3 and c_4 , the transfer is slower than that predicted by the simple no-fringe-field theory, curve

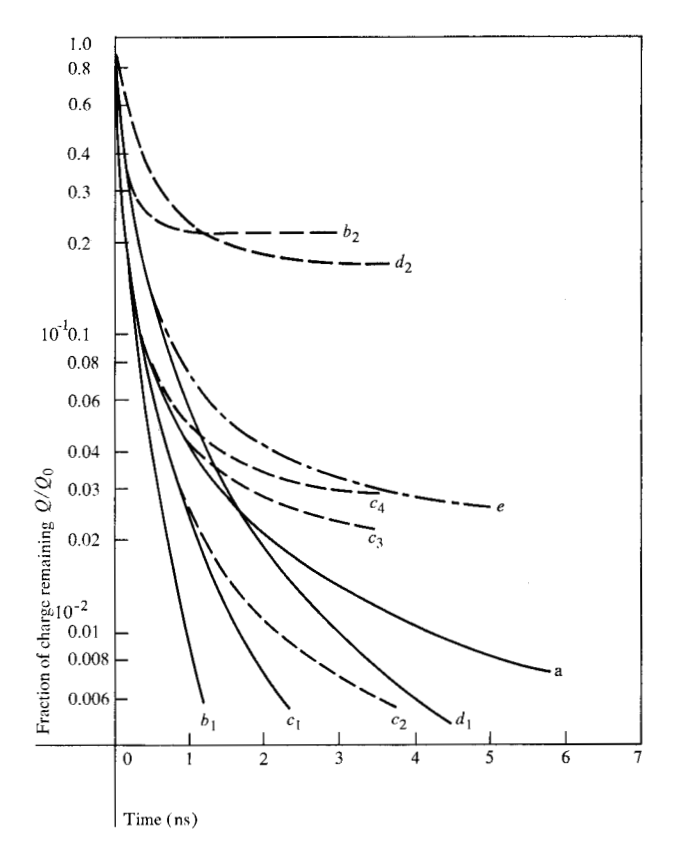


Figure 2 The transfer efficiency of a CCD. $W^* = 5 \mu m$, $N_A^* = 5 \times 10^{15} / \text{cm}^3$, $\mu_0^* = 400 \text{ cm}^2 / \text{V-s}$. (a) Simple theory (Strain and

Schryer), $Sq_0 = 10 \text{ V}$. (b) and (c) $h_1^* \uparrow h_2^* / h_2^*$ (b₁) $h_1^* = 2000 \text{ Å}$, $h_2^* = 1000 \text{ Å}$, $V_1^* = 13 \text{ V}$, $V_2^* = 23 \text{ V}$ $n^* = 0.96 \times 10^{12}/\text{cm}^2$, $n_s^* = 10^{11}/\text{cm}^2$. (b₂) Same as (b₁), except $h_1^* = 1000 \text{ Å}$, $h_2^* = 2000 \text{ Å}$. (c₁) $h_1^* = 1000 \text{ Å}$, $h_2^* = 2000 \text{ Å}$, $V_1^* = 11 \text{ V}$, $V_2^* = 35 \text{ V}$, $n^* = 1.6 \times 10^{12}/\text{cm}^2$, $n_s^* = 10^{11}/\text{cm}^2$. (c₂) Same as (c₁), except $V_2^* = 33 \text{ V}$. (c₃) Same as (c₁), except $V_2^* = 31.5 \text{ V}$. (c₄) Same as (c₁), except $V_2^* = 31 \text{ V}$. (d) and (e):

$$\begin{array}{c|c}
V_1^* & V_2^* \\
|\leftarrow W \rightarrow |\leftarrow 2\mu \rightarrow |\leftarrow W \rightarrow | \\
\hline
\end{array}$$

$$W = 5 \mu \text{m.}$$
1000 Å

 $(d_1) V_1^* = 9 V, V_2^* = 24 V. (d_2) V_1^* = 9 V, V_2^* = 18 V. (e) n^* = 1.51 \times 10^{12} / \text{cm}^2, n_2^* = 3 \times 10^{11} / \text{cm}^2, V_1^* = 8 V, V_2^* = 17 V.$

a. The simple theory gives a good qualitative result, although it is not adequate to predict the detailed transfer in view of the large variation of results obtained. To obtain a speedy transfer, a moderate potential difference must be maintained between the two adjacent potential wells. When charge is transferred to a low capacitance region from a high capacitance region, the surface potential variation in the lower capacitance region is larger than that in the higher capacitance region; thus it tends to re-

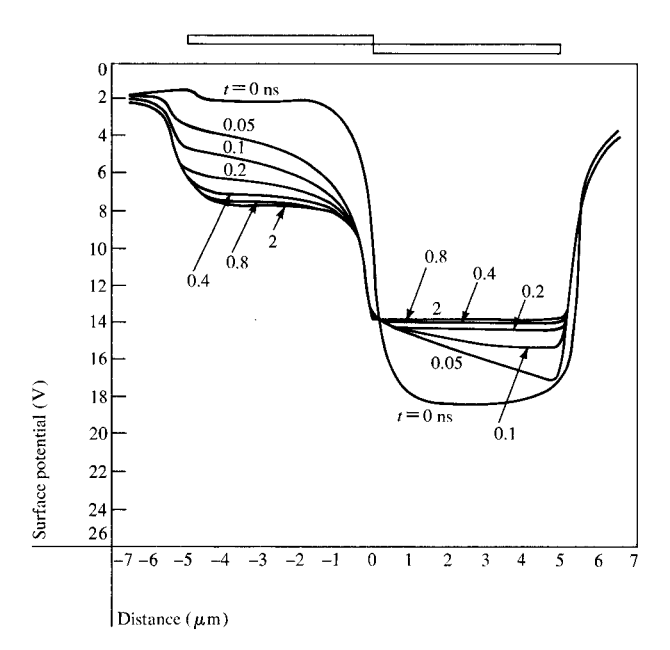
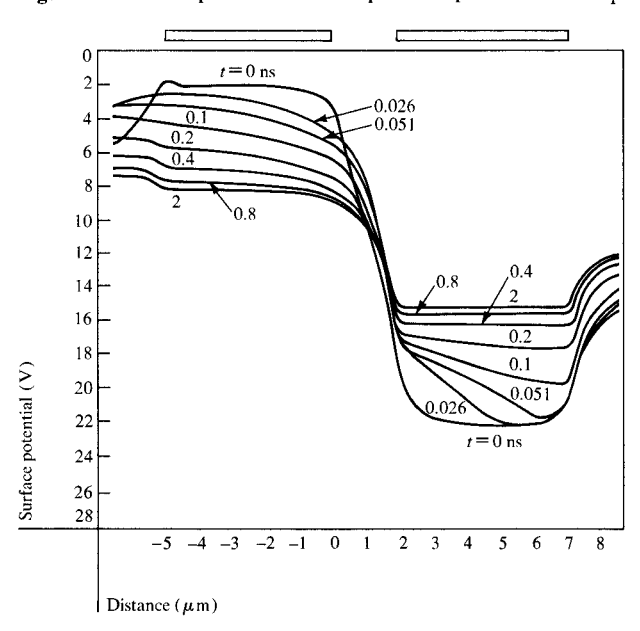


Figure 3 Time dependence surface potential profile for case b₁.





duce the effective driving field and causes the transfer to slow down. This fact can be seen more clearly in a gapped structure. Curves d_1 , d_2 and e (Fig. 2) indicate the results calculated for a device with a 2- μ m gap. The oxide thickness is 1000 Å. No surface state charge is assumed for cases d_1 and d_2 . The charge density again is $Sq_0=10$ V. The applied voltages in d_1 are 9 V and 24 V. From d_1 , the transfer is seen to be slower initially, but the transfer rate is speeded up later by the surface field. Figure 5 shows the surface potential distribution as a function of

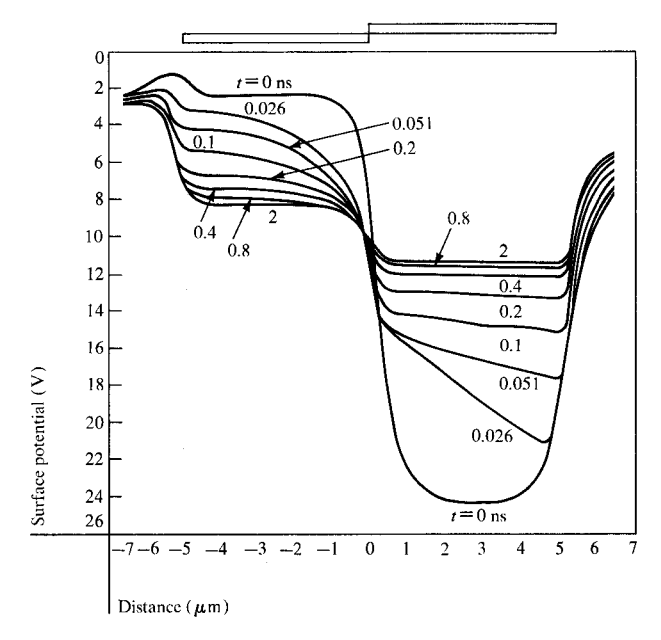


Figure 4 Time dependence surface potential profile for case c₁.

time for d₁. The initial transfer is slowed down by the fact that part of the charges have to be moved backward initially and, more importantly, the effective channel length is moved considerably outward into the gap. Unless the amount of surface field in the gap region is extremely large, the effective channel length is lengthened and the device behaves as a longer electrode device. It is interesting to note that if the effective channel length is taken to be 7 μ m (the combined length of the electrode and the gap), and if the time is multiplied by $(5/7)^2$ so that the transfer characteristic corresponds to a 5 µm device, the transfer would follow roughly along curve c₁. If the receiving potential well, being filled up by the transferred charge, approaches the source potential well, the effective channel length would be further lengthened and the transfer slowed down more. Eventually a potential barrier may form and the remaining charge is trapped. Curve d, shows such a case with a potential barrier in the gap. The barrier can be lowered or eliminated with a higher concentration of surface-state charge. An example is given in curve e. In practice, however, such a high density of surface state charge in some cases can not be tolerated. When this is true, a higher gate voltage or a smaller gap is required to eliminate the barrier. From Fig. 2, even though we have used a doping concentration of 5×10^{15} / cm³, the transfer characteristics of the device are seen to be modified greatly by the amount of total existing field due to the different electrode configuration and the applied voltages.

If a lighter doping, such as that employed by Amelio [23] is used, the amount of total field will increase, and its effect on the device transfer characteristic will be even

more pronounced. In the above example, all voltages are assumed to be applied suddenly at t=0. An example of time-dependent applied voltages is given in Fig. 6 for a three-electrode CCD. The cusp of the curve is due to backflow of charges from gate 2 into gate 1. The inclusion of field-dependent mobility in the analysis slightly slows down the transfer, but the overall characteristic remains unchanged.

Summary

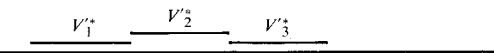
A detailed analysis of CCD charge transfer has been described. The analysis is based on solving the transport equation with the actual time-dependent surface field calculated for a practical CCD structure. Devices with different oxide thicknesses and devices with electrode gaps have been examined. It is found that the net surface field plays an important role in all cases studied. The effective channel length is found to be modulated by the net surface field and depends on the electrode configuration of the device. When charge is transferred from a low oxide capacitance region into a high oxide capacitance region, the effective channel length is shortest and the transfer fastest for the cases studied. The transfer is slowest for a gapped device with the same electrode length. The effective channel length of the gapped device can be varied from about one electrode length to roughly a combined length of the electrode and the gap, depending on the amount of net field present in the gap as a function of time. In view of the large variation of results obtained, the simple one-dimensional analysis must be used with some caution.

Acknowledgment

The authors thank Dr. H. S. Lee for many stimulating discussions during the course of this investigation.

References

- W. S. Boyle and G. E. Smith, "Charge Coupled Semiconductor Devices," Bell Syst. Tech. J. 49, 587 (1970).
- B. J. Strain and N. L. Schryer, "A Nonlinear Diffusion Analysis of Charge-Coupled-Device Transfer," Bell Syst. Tech. J. 50, 1721 (1971).
- 3. C. K. Kim and M. Lenzlinger, "Charge Transfer in Charge-Coupled Devices," *J. Appl. Phys.* 42, 3586 (1971).
- 4. L. G. Heller, W. H. Chang and A. W. Lo, "A Model of Charge Transfer in Bucket Brigade and Charge-Coupled Devices," *IBM J. Res. Develop.* 16, 184 (1972).
- J. E. Carnes, W. F. Kosonocky and E. G. Ramberg, "Drift-Aiding Fringing Fields in Charge-Coupled Devices," *IEEE J. Solid-State Circuits* SC-6, 322 (1971).
- W. E. Engeler, J. J. Tiemann and R. D. Baertsch, "Surface Charge Transport in Silicon," Appl. Physics Lett. 17, 469 (1971).
- 7. W. B. Joyce and W. J. Bertram, "Linearized Dispersion Relation and Green's Function for Discrete-Charge-Transfer Devices with Incomplete Transfer," *Bell Syst. Tech. J.* 50, 1741 (1971).
- R. H. Krambeck, "Zero Loss Transfer Across Gaps in CCD," Bell Syst. Tech. J. 50, 3169 (1971).



 $W^* = 5 \mu m, h_1^2 = h_3^* = 1000 \text{Å}, h_2 = 2000 \text{Å}, N_A^* = 5 \times 10^{15} / \text{cm}^3$ $\mu_0^* = 400 \text{ cm}^2 / \text{v} - \text{s}, n_s^* = 10^{11} / \text{cm}^2, n^* = 1.66 \times 10^{12} / \text{cm}^2$

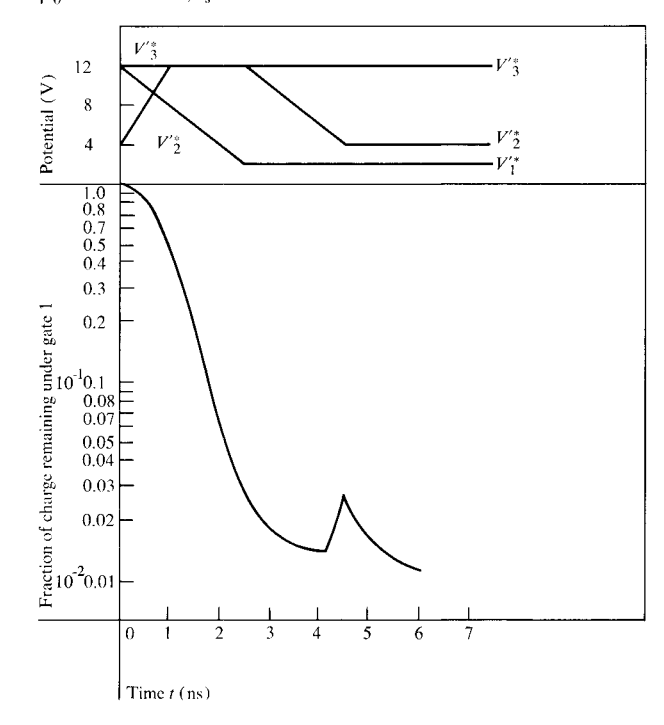


Figure 6 Charge transfer characteristics of a three-electrode CCD.

- 9. H. S. Lee and L. G. Heller, "Charge-Control Method of Charge-Coupled-Device Transfer Analysis," *IEEE Trans. Electron Devices* **ED-19**, 1270 (1972).
- G. F. Amelio, M. F. Tompsett and G. E. Smith, "Experimental Verification of Charge Coupled Device Concept," *Bell Syst. Tech. J.* 49, 593 (1970).
- M. F. Tompsett, G. F. Amelio and G. E. Smith, "Charge Coupled 8-Bit Shift Register," Appl. Physics Lett. 17, 111 (1970).
- W. E. Engeler, J. J. Tiemann and R. D. Baertsch, "The Surface-Charge Transistor," *IEEE Trans. Electron Devices* ED-18, 1125 (1971).
- C. N. Berglund and R. J. Strain, "Fabrication and Performance Considerations of Charge-Transfer Dynamic Shift Registers," Bell Syst. Tech. J. 51, 655, (1972).
- W. E. Engeler, J. J. Tiemann and R. D. Baertsch, "Surface-Charge Transport in a Multielement Charge-Transfer Structure," J. Appl. Phys. 43, 2277 (1972).
- A. M. Mohsen, T. C. McGill and C. A. Mead, "Charge Transfer in Overlapping Gate Charge-Coupled Devices," IEEE J. Solid-State Circuits SC-8, 191 (1973).
- W. F. Kosonocky and J. E. Carnes, "Charge-Coupled Digital Circuits," *IEEE J. Solid-State Circuits* SC-6, 314 (1971).
- W. E. Engeler, J. J. Tiemann and R. D. Baertsch, "A Memory System Based on Surface-Charge Transport," *IEEE J. Solid-State Circuits* SC-6, 306 (1971).
- 18. N. G. Vogl and T. V. Harroun, 1972 International Solid-State Circuit Conference Digest, 16, 246 (1972).
- N. A. Patrin, A. Bhattacharyya, M. L. Joshi and J. J. Chang, IEEE NEREM Record 14, 157 (1972).

441

- N. A. Patrin, "Performance of Very High Density Charge Coupled Devices," IBM J. Res. Develop. 17, 241 (1973).
 G. F. Amelio, W. J. Bertram, Jr. and M. F. Tompsett,
- G. F. Amelio, W. J. Bertram, Jr. and M. F. Tompsett, "Charge-Coupled Imaging Devices: Design Considerations," *IEEE Trans. Electron Devices* ED-18, 986 (1971).
 M. F. Tompsett, G. F. Amelio, W. J. Bertram, Jr., R. R.
- M. F. Tompsett, G. F. Amelio, W. J. Bertram, Jr., R. R. Buckley, W. J. McNamara, J. C. Mikkelsen, Jr. and D. A. Sealer, "Charge-Coupled Imaging Devices: Experimental Results," *IEEE Trans. Electron Devices* ED-18, 992 (1971).
- 23. G. F. Amelio, "Computer Modelling of Charge-Coupled Device Characteristics," *Bell Syst. Tech. J.* 51, 705 (1972).
- 24. J. E. Carnes, W. F. Kosonocky and E. G. Ramberg, "Free Charge Transfer in Charge-Coupled Devices," *IEEE Trans Electron Devices* **ED-19**, 798 (1972).

25. W. H. Chang and H. S. Lee, "Potential Distribution of an Inhomogeneously Doped MIS Array," *IBM J. Res. Develop.* 18, 47 (1974).

Received February 27, 1974.

The authors are located at the IBM System Products Division Laboratory at Burlington, P.O. Box 4, Essex Junction, Vermont 05452.